

# Domain-Decomposition Technique for Efficient Analysis of Rotationally Symmetric Reflector Systems Containing 3D Structures

Erik Jørgensen and Peter Meincke  
TICRA

Læderstræde 34, DK-1201 Copenhagen K, Denmark  
Email: ej@ticra.com, pme@ticra.com

**Abstract**—An efficient algorithm for analysis and optimization of rotationally symmetric reflector antennas, possibly including 3D support structures and/or waveguide components, is presented. The high efficiency is obtained by using a domain-decomposition approach where each region of space is characterized independently using a generalized admittance matrix description. The admittance matrices are obtained using circular mode-matching, higher-order 3D MoM, or a newly developed higher-order MoM for bodies of revolution (BoR-MoM). The antenna performance is rigorously evaluated by cascading the admittance matrices, which subsequently allows computation of surface currents or fields in all subdomains. The new algorithm allows fast and accurate analysis and optimization of rotationally symmetric reflectors, even in cases that would normally require a time-consuming 3D solution due to the lack of rotational symmetry.

**Index Terms**—Rotationally symmetric reflectors, body of revolution, higher-order MoM, domain decomposition, generalized admittance matrix

## I. INTRODUCTION

Rotationally symmetric reflector systems are attractive candidates for realizing low-cost compact high-gain antennas with low sidelobes and low cross polarization. These compact reflector systems often employ two reflectors in a classical axially displaced reflector configuration [1], or alternatively, a single reflector with a backward radiating hat feed or splash-plate feed [2], [3]. A common feature of these antennas is a tight integration of feed, feed hat or subreflector, dielectric support structure, and main reflector, resulting in a highly resonant structure. In addition, many terminal antennas based on rotationally symmetric reflectors include 3D structures, e.g., waveguide components with arbitrary cross section or metallic struts. A typical example of such an antenna was presented in [4] where the presence of four metallic struts and 3D corrugations precluded the use of rotational symmetry. The highly resonant structure and the lack of symmetry often leave a relatively slow 3D full-wave analysis as the only option, thus prohibiting efficient numerical optimization of the antenna performance.

In this paper, we propose a domain-decomposition technique allowing different analysis methods to be used in different regions of space. With this technique, the rotationally symmetric parts of the antenna system – usually constituting

the largest part of the antenna – can be analyzed with a Body-of-Revolution Method of Moments (BoR-MoM) solver and the remaining 3D parts can be analyzed with 3D-MoM. The technique allows multiple BoR-MoM and 3D-MoM regions and the region boundaries may intersect the antenna geometry. In addition, the technique also includes mode-matching for circular waveguides and horns.

The domain-decomposition technique is combined with a generalized admittance matrix framework, where the admittance matrix of each subdomain is extracted by defining equivalent magnetic port expansion currents on the domain boundaries. The overall admittance matrix is obtained by using standard techniques for cascading of admittance matrices. When the excitation is known, the fields and currents may finally be computed everywhere. The admittance matrix approach allows a flexible choice of solver in each domain as well as a very fast evaluation of the antenna performance during a numerical optimization procedure. This is accomplished by reusing the admittance matrices of the unchanged parts and rebuilding the full-wave solution. As an example, the admittance matrix of the main reflector is reused when the shape of the subreflector is optimized. By combining the domain-decomposition approach with a higher-order BoR-MoM solver, we show that analysis of typical hat-feed antennas is performed in 1-2 seconds on a laptop, whereas the time to rebuild the full solution during a numerical optimization is measured in fractions of a second.

The paper is organized as follows: Section II reviews a recently developed higher-order version of the BoR-MoM that reduces the number of unknowns significantly when compared to the commonly applied low-order solution [5]. Section III introduces the domain-decomposition scheme and the extraction of scattering matrices is discussed in Section III-A. Finally, numerical results will be shown to illustrate the speed and accuracy of the approach.

## II. HIGHER-ORDER BOR-MOM

The BoR-MoM has been formulated previously in several works [5]-[7]. All these works have employed triangular basis functions on flat curve segments which typically requires 15 unknowns per wavelength to achieve accurate results. This leads to a typical analysis time of 30-60 seconds per frequency

point for a compact hat-feed antenna. In this work, we use a more advanced discretization scheme derived from the 3D higher-order basis functions presented in [8]. The electric and magnetic surface currents on each curve segment are expanded as

$$\mathbf{X} = \sum_{m=0}^{M^\phi} \sum_{n=0}^{N^t} a_{mn}^{t,e} \mathbf{B}_{mn}^{t,e} + a_{mn}^{t,o} \mathbf{B}_{mn}^{t,o} + \sum_{m=0}^{M^\phi} \sum_{n=0}^{N^t-1} a_{mn}^{\phi,e} \mathbf{B}_{mn}^{\phi,e} + a_{mn}^{\phi,o} \mathbf{B}_{mn}^{\phi,o}, \quad (1)$$

where  $\mathbf{X} = \mathbf{J}, \mathbf{M}$ ,  $a_{mn}^{t,e}$ ,  $a_{mn}^{t,o}$ ,  $a_{mn}^{\phi,e}$ , and  $a_{mn}^{\phi,o}$  are unknown coefficients,  $N^t$  is the polynomial expansion order along the generatrix,  $M^\phi$  is the azimuthal mode index, and  $\mathbf{B}_{mn}^{t,e}$ ,  $\mathbf{B}_{mn}^{t,o}$ ,  $\mathbf{B}_{mn}^{\phi,e}$ , and  $\mathbf{B}_{mn}^{\phi,o}$  are  $t$ - and  $\phi$ -directed vector basis function defined as

$$\mathbf{B}_{mn}^{t,(e)}(t, \phi) = \frac{\mathbf{a}_t}{\mathcal{J}_s(t, \phi)} \tilde{P}_n(t) \begin{pmatrix} \cos m\phi \\ \sin m\phi \end{pmatrix}, \quad (2a)$$

$$\mathbf{B}_{mn}^{\phi,(e)}(t, \phi) = \frac{\mathbf{a}_\phi}{\mathcal{J}_s(t, \phi)} P_n(t) \begin{pmatrix} \cos m\phi \\ \sin m\phi \end{pmatrix}, \quad (2b)$$

where  $\mathbf{a}_t = \partial \mathbf{r} / \partial t$ ,  $\mathbf{a}_\phi = \partial \mathbf{r} / \partial \phi$ , and  $\mathcal{J}_s(t, \phi) = |\mathbf{a}_t \times \mathbf{a}_\phi|$ . In Eq. (2b), the polynomials  $P_n$  are Legendre polynomials and in Eq. (2a), modified Legendre polynomials  $\tilde{P}_n$  are used to allow the current continuity to be enforced [8]. The modal expansion order,  $M^\phi$ , should be adjusted to the specific problem. The expansion order along the generatrix,  $N^t$ , is adapted to the electrical length of each segment which is usually in the order of  $2\lambda$ . The BoR patches, obtained by rotation of a single curved segment around the  $z$ -axis, are illustrated in Fig. 1 for the case of 1st, 2nd, and 3rd order segments. When higher-order basis functions and curved segments are used, the number of unknowns is reduced by a factor of 4 and drops to about 3-4 per wavelength, implying that the system matrix is easily stored and inverted, even for structures larger than several hundred wavelengths. The bottleneck for smaller problems is usually the matrix fill time which, however, can be dramatically reduced by using analytical techniques [9].



Fig. 1. Surfaces realized using a single BoR patch of first (left), second (centre), and third order (right), respectively. The generatrix is described by a Lagrange polynomial passing through 2, 3, or 4 interpolation nodes, respectively. The cubic patches using 4 interpolation nodes per patch generally provides the highest accuracy for curved surfaces and is preferred for reflectors.

### III. DOMAIN DECOMPOSITION ALGORITHM

Analysis and optimization of waveguide devices are routinely performed by computing scattering or admittance matrices of each component separately and using a cascading procedure to obtain the overall system response. This rigorous approach has the following advantages:

- 1) The computational cost of solving multiple small problems, and using cascading, is usually much lower than the cost required for solving one large problem.
- 2) Each component may be analyzed and optimized independently using the optimal analysis algorithm for the component in question.
- 3) When optimizing a system composed of multiple components, only the component being changed needs to be re-analyzed. The time to assemble the full solution is then a fraction of the time used for the initial analysis of the system.

For waveguide devices, the different components can be decoupled by introducing a number of waveguide ports with an associated set of port expansion functions. The port expansion functions are usually chosen as the eigenvectors of a waveguide with the same cross section as the waveguide port. This choice leads to relative small scattering or admittance matrices as well as high accuracy.

The scattering/admittance matrix method described above may equally well be applied to a free-space region with a number of isolated or connected scatterers. The free-space region is then divided into a number of subdomains, and each subdomain is enclosed by a port surface with suitable port expansion functions for the field. The advantages listed in the previous paragraph still hold for this approach. However, only a limited number of works have attempted such a solution, e.g., [10] for the case of coupling between a feed and a reflector, [11] for an antenna placement problem, or [12] for antennas in arbitrary environments. These works have employed spherical vector waves as port expansion functions, leading to a relatively compact scattering or admittance matrix. However, the use of spherical vector waves implies that only spherical port surfaces may be used. This is a severe limitation for closely separated or connected scatterers.

In the present work, we use an admittance matrix description of a region of space that may contain one or more scatterers and one or more waveguide apertures. The region is enclosed by a number of port surfaces and these ports are denoted radiation ports. The geometry of the radiation port may be represented as a surface mesh and standard MoM basis functions are used as port expansion functions, thereby eliminating the above-mentioned problems of previous works based on spherical vector waves. The radiation ports enclosing the region, and optionally the waveguide apertures or a conducting part of a scatterer, must define a single closed surface that act as a boundary of the region being characterized. Alternatively, the region may be defined by the space outside a closed surface and extending to infinity. The admittance matrix of each region is obtained by MoM as described below and the choice of port geometry and associated port expansion functions is addressed in Section III-B. Once all admittance matrices are known, standard techniques for cascading of admittance matrices are employed to eliminate all internal ports. This procedure leaves only a waveguide port at the horn throat where the desired excitation can be applied.

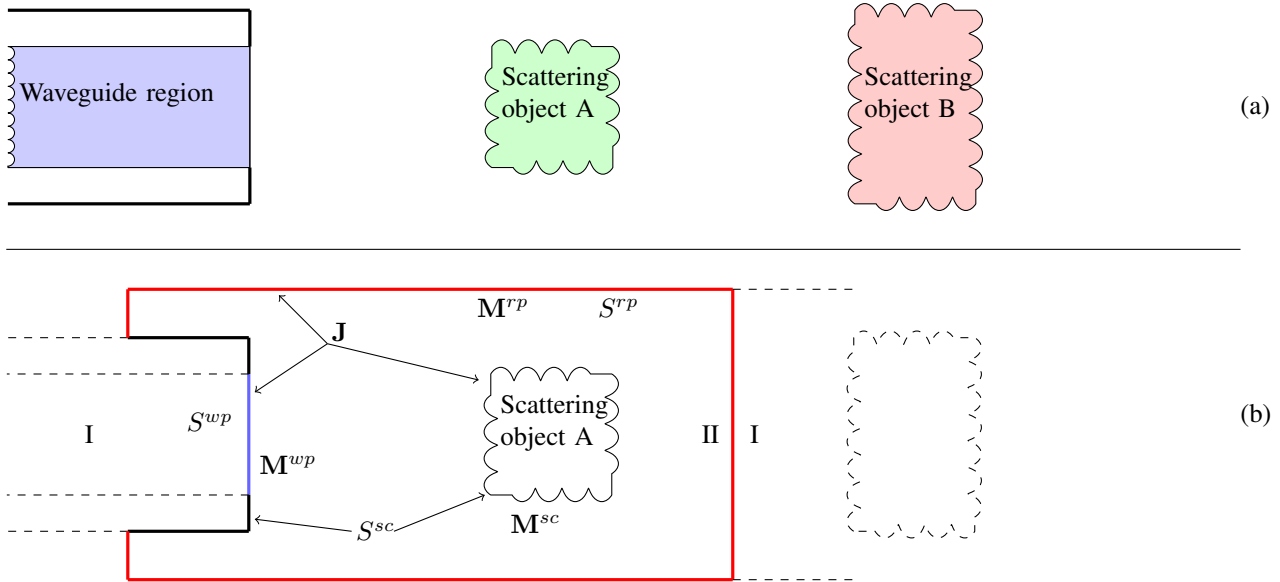


Fig. 2. Top: A horn aperture is illuminating two scattering objects. Bottom: Equivalent problem for extraction of the admittance matrix of the region containing object A. The aperture is closed by a waveguide port defined on the blue surface  $S^{wp}$ . The surface of object A and the outer waveguide wall is denoted  $S^{sc}$ . The region is bounded by a radiation port located in free space. The surface of this radiation port is denoted  $S^{rp}$  and is shown in red. The waveguide port and the radiation port is closed by a PEC surface. Electric MoM basis functions  $\mathbf{J}$  are defined on the surface  $S^{sc} + S^{wp} + S^{rp}$ , magnetic waveguide port basis functions  $\mathbf{M}^{wp}$  are defined on  $S^{wp}$ , magnetic radiation port basis functions  $\mathbf{M}^{rp}$  are defined on  $S^{rp}$ , and magnetic MoM basis functions  $\mathbf{M}^{sc}$  are defined on the dielectric parts of the scattering object. The space outside the region containing scatterer A is denoted region I and the space inside is denoted region II.

### A. Extraction of Admittance Matrices

The admittance matrix of an arbitrarily shaped closed waveguide region with  $N$  waveguide ports can be obtained by MoM [13]. In the present work, we use a similar approach for extracting the admittance matrix of a region enclosed by multiple waveguide and radiation ports [14]. The region may contain one or more composite metallic/dielectric scatterers. Consider the geometry in Fig. 2(a) showing a waveguide aperture illuminating two scatterers (A and B). We wish to obtain an admittance matrix of the region containing the waveguide aperture and scatterer A. To this end, we introduce the radiation port shown with a red line in Fig. 2(b) and the waveguide port shown with a blue line. The region is now bounded by a closed surface consisting of the red and the blue surfaces, as well as a part of the exterior waveguide wall, which is considered to be a part of the scatterer. The space outside the region containing scatterer A is denoted region I and the space inside is denoted region II. In the following we assume that an impressed field may exist in region I. By using the surface equivalence principle, we close the port boundaries, denoted  $S^p = S^{rp} + S^{wp}$ , by a PEC surface and define equivalent magnetic port currents on this surface as  $\mathbf{M}^p(\mathbf{r}) = -\hat{n} \times \mathbf{E}(\mathbf{r})$ , where  $\hat{n}$  is a unit normal directed from region I into region II. The continuity of the magnetic field at the port interface requires

$$\mathbf{H}_{\tan}^I(-\mathbf{M}^p) + \mathbf{H}_{\tan}^i = \mathbf{H}_{\tan}^{II}(\mathbf{M}^p), \quad (3)$$

where  $\mathbf{H}^I(-\mathbf{M}^p)$ ,  $\mathbf{H}^{II}(\mathbf{M}^p)$  denote the magnetic field radiated in regions I and II, respectively, and  $\mathbf{H}^i$  is the impressed magnetic field in region I. The magnetic port current is now

expanded as

$$\mathbf{M}^p(\mathbf{r}) = \eta_0 \sum_{i=1}^{N^p} V_i \mathbf{M}_i^p, \quad (4)$$

where  $\eta_0$  is the free space impedance and  $N^p$  is the number of port expansion function. By choosing  $N^p$  port weighting functions  $\mathbf{W}_j^p$  and forming inner product with (3), we obtain the matrix equation

$$[I^p] = [Y^I + Y^{II}] [V] \quad (5)$$

in which  $[I^p]$  is related to the impressed field as

$$[I^p] = [\langle \mathbf{W}_j^p; \mathbf{H}_{\tan}^i \rangle], \quad j = 1, \dots, N^p \quad (6)$$

and  $[Y^{I,II}]$  are the normalised admittance matrices

$$[Y^{I,II}] = \eta_0 [\langle \mathbf{W}_j^p; \mathbf{H}_{\tan}^{I,II}(\mathbf{M}_i^p) \rangle]. \quad (7)$$

In [14], we showed that the admittance matrix  $[Y^{II}]$ , that fully characterizes region II, can be obtained as

$$[Y^{II}] = [Q] [Z]^{-1} [P], \text{ with} \quad (8)$$

$$[Q] = \langle \mathbf{W}_j^p; -\hat{n} \times \mathbf{J}_t \rangle, \quad (9)$$

$$[P] = \left\langle \mathbf{T}_s; \hat{n} \times \mathbf{M}_i^p + \nabla \times \int_{S^p} \mathbf{M}_i^p G dS' \right\rangle, \text{ and} \quad (10)$$

$$[Z] = \frac{-j}{k_0} \left\langle \mathbf{T}_s; \nabla \times \nabla \times \int_{S^p + S^{sc}} \mathbf{J}_t G dS' \right\rangle. \quad (11)$$

In these expressions,  $\mathbf{W}_j^p$  are port weighting functions usually chosen as  $\mathbf{W}_j^p = \mathbf{M}^p$ ,  $\mathbf{J}_t$  are MoM basis functions, and  $\mathbf{T}_s$  are MoM weighting functions usually chosen as  $\mathbf{T}_s = \mathbf{J}_t$ .

### B. Choice of Port Geometry and Expansion functions

The domain decomposition approach employs two port types: Waveguide ports and radiation ports. For waveguide ports, the port expansion functions are chosen as  $\hat{n} \times \mathbf{e}_{mn}$  where  $\hat{n}$  is a unit normal vector to the port and  $\mathbf{e}_{mn}$  are the orthonormal electric eigenvectors of the waveguide. For radiation ports, we have chosen to use the BoR patches in Fig. 1 and the basis functions in Eq. (2) to represent the port geometry and the port expansion functions, respectively. This choice results in a very low number of port expansion functions and consequently a compact admittance matrix. In addition, the admittance matrix of a circular symmetric region is a block-diagonal matrix where each block corresponds to a single azimuthal  $m$ -index that may be computed and stored separately. The selected radiation port geometry is ideally suited for rotationally symmetric reflectors as illustrated by the two examples in Fig. 3. The key point is that the BoR-MoM can be used for the electrically large main reflector even if one of the blue regions contains a 3D structure.

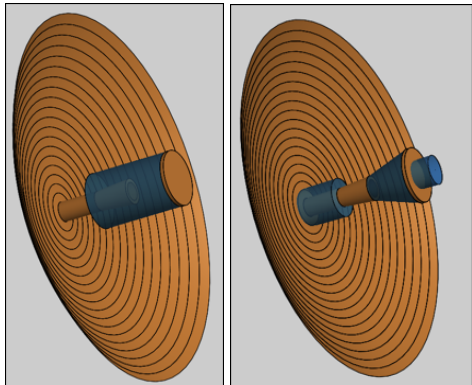


Fig. 3. Illustration of domain-decomposition approach with radiation port surfaces shown in transparent blue. Left: Simple subdivision; front of subreflector and horn aperture are inside one domain, rear of subreflector and main reflector are in the exterior domain extending to infinity. Right: Complex sub-division with additional domains, e.g., for optimization of the subreflector support structure, an additional antenna mounted behind the sub, or for optimization of a Gaussian vertex plate [15].

## IV. NUMERICAL RESULTS

The new BoR-MoM algorithm presented in Section II provides fast analysis of large rotationally symmetric reflectors. Example run-times for a canonical ring-focus geometry are reported in Fig. 4 - these results are obtained on a laptop without using the new domain-decomposition technique. Figure 5 shows a test geometry consisting of a corrugated horn with 75 corrugations,  $11\lambda$  subreflector, and  $70\lambda$  main reflector. The front of the subreflector is now enclosed in a radiation port, which has been chosen to allow rapid shaping of the subreflector. This configuration involves three domains:

- 1) horn interior,
- 2) front of subreflector, and
- 3) horn aperture, subreflector rear part, and main reflector.

The new domain-decomposition scheme has then been tested using various combinations of solvers. In particular, mode-

Main reflector diameter	Computation time
$15\lambda$	0.2 s
$25\lambda$	0.3 s
$40\lambda$	0.7 s
$50\lambda$	1.2 s
$75\lambda$	3.0 s
$100\lambda$	5.7 s

Fig. 4. Higher-order BoR-MoM computation times for a simple ring-focus reflector antenna, (laptop computer, 2011 model). The antenna geometry comprises a main reflector, a subreflector, and the exterior waveguide wall. The horn is a simple open-ended waveguide and the reported computation time includes extraction of waveguide scattering parameters. The computation time per frequency is listed for antennas of different sizes.

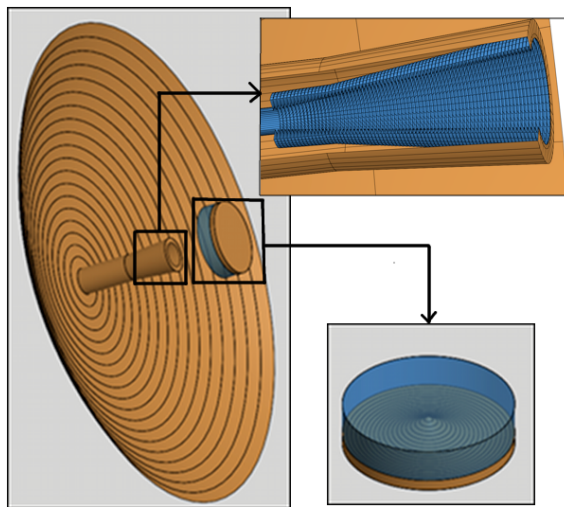


Fig. 5. Ring-focus test geometry: Corrugated horn with 75 corrugations,  $11\lambda$  subreflector with finite thickness, and  $70\lambda$  main reflector. The front of the subreflector is located inside a small domain bounded by the transparent blue radiation port surface.

matching and BoR-MoM in domain 1, BoR-MoM and 3D MoM in domain 2, and BoR-MoM in domain 3. The results were compared to a standard coupled mode-matching/BoR-MoM algorithm and all methods produced essentially identical results, thus illustrating that the approach presented here is rigorous. The excellent agreement can be seen in Fig. 6, that shows two curves obtained with the standard mode-matching/BoR-MoM solution, as well as with the new method using BoR-MoM in domains 2 and 3.

The radiation port geometry in the example above allows rapid shaping of the subreflector. In each cost function evaluation, it is sufficient to recompute the admittance matrix of the small domain containing the front of the subreflector. The computation time is reported in Table I where it is observed that the initial run of the domain-decomposition method is slightly slower than the standard solution, but the subsequent

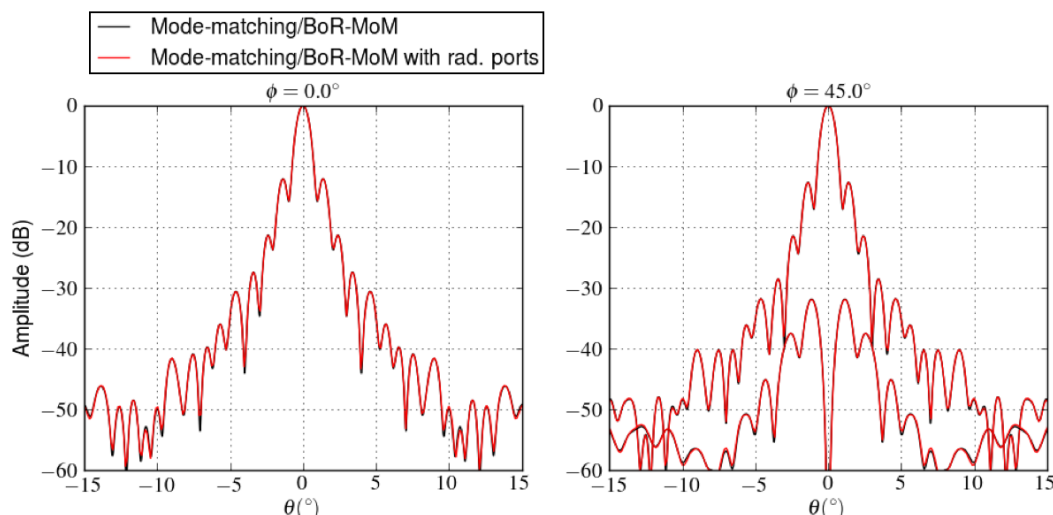


Fig. 6. Far-field pattern of the test geometry shown in Fig. 5. Patterns have been obtained with a standard coupled mode-matching/BoR-MoM solution as well as the domain-decomposition approach using multiple BoR-MoM domains separated by radiation ports.

recomputation using a new subreflector can be accomplished an order of magnitude faster than the standard solution. In this case the recomputation time was reduced to 0.3 seconds.

TABLE I  
RELATIVE COMPUTATION TIMES PER FREQUENCY POINT FOR THE ANTENNA SHOWN IN FIG. 5.

Full mode-matching/BoR-MoM)	1.0
First run of domain-decomposition algorithm with radiation ports	1.26
Subsequent runs of domain-decomposition algorithm with radiation ports	0.11

## V. CONCLUSION

We have presented a domain-decomposition method based on generalized admittance matrices and higher-order MoM. The method allows 3D-MoM to be used for in regions with no symmetry, whereas the fast BoR-MoM can be used for the rotationally symmetric parts. In addition, we showed that the method allows fast recomputation of the full-wave solution when a geometrical change has been introduced in one of the subdomains, thus making the method ideally suited for optimization of rotationally symmetric reflector systems. Additional numerical results and comparison with measurements will be presented at the conference.

## ACKNOWLEDGMENT

This work is partially funded by ESA/ESTEC, ESTEC contract 4000104664/11/NL/US, and by the Danish National Advanced Technology Foundation, j.nr. 004-2010-1.

## REFERENCES

- [1] F. J. S. Moreira and A. Prata, "Generalized classical axially symmetric dual-reflector antennas," *IEEE Trans. Antennas Propagat.*, vol. 49, no. 4, pp. 547–554, April 2001.
- [2] P.-S. Kildal, "The hat feed: a dual-mode rear-radiating waveguide antenna having low cross polarization," *IEEE Trans. Antennas Propagat.*, vol. AP-35, no. 9, pp. 1010–1016, 1987.
- [3] E. G. Geterud, J. Yang, T. Ostling, and P. Bergmark, "Design and optimization of a compact wideband hat-fed reflector antenna for satellite communications," *IEEE Trans. Antennas Propagat.*, vol. 61, pp. 125 – 133, 2013.
- [4] J. Yang, W. Wei, T. Ostling, and T. Schafer, "A new metal-rod-supported hat antenna for potentially combining with the eleven antenna as a dual-band feed for reflectors," in *European Conference on Antennas and Propagation, EuCAP*, 2011.
- [5] J. R. Mautz and R. F. Harrington, "H-field, E-field, and combined field solutions for bodies of revolution," Syracuse University, NY, USA, Tech. Rep. TR-77-2, Feb. 1977.
- [6] T. K. Wu and L. L. Tsai, "Scattering from arbitrarily-shaped lossy dielectric bodies of revolution," *Radio Sci.*, vol. 12, pp. 709–718, 1977.
- [7] A. A. Kishk and L. Shafai, "Different formulations for numerical solution of single or multibodies of revolution with mixed boundary conditions," *IEEE Trans. Antennas Propagat.*, vol. 34, no. 5, pp. 666–673, 1986.
- [8] E. Jørgensen, J. L. Volakis, P. Meincke, and O. Breinbjerg, "Higher order hierarchical Legendre basis functions for electromagnetic modeling," *IEEE Trans. Antennas Propagat.*, vol. 52, no. 11, pp. 2985–2995, Nov. 2004.
- [9] M. Gustafsson, "Accurate and efficient evaluation of modal green's functions," *Journal of Electromagnetic Waves and Applications*, vol. 24, no. 10, pp. 1291–1301, 2010.
- [10] C. D. Giovampaola, E. Martini, A. Toccafondi, and S. Maci, "Antenna mismatch induced by nearby scatterers through a spherical wave - generalized scattering matrix approach," *Electromagnetic Theory (EMTS), 2010 URSI International Symposium on*, pp. 776 – 779, 2010.
- [11] A. Barka and P. Caudrillier, "Domain decomposition method based on generalized scattering matrix for installed performance of antennas on aircraft," *IEEE Trans. Antennas Propagat.*, vol. 55, no. 6, pp. 1833 – 1842, 2007.
- [12] R. J. Pirkel, "Spherical wave scattering matrix description of antenna coupling in arbitrary environments," *IEEE Trans. Antennas Propagat.*, vol. 60, no. 12, pp. 5654–5662, Dec. 2012.
- [13] R. Bunger and F. Arndt, "Moment-method analysis of arbitrary 3-d metallic n-port waveguide structures," *IEEE Trans. Microwave Theory and Techniques*, vol. 48, no. 4, pp. 531 – 537, 2000.
- [14] E. Jørgensen, P. Meincke, and S. Sabbadini, "Fast and accurate design tool for rotationally symmetric reflector antennas with 3d waveguide components and support structures," in *Proc. 34th ESA Antenna Workshop*, Noordwijk, The Netherlands, 2012.
- [15] J. Yang and P.-S. Kildal, "Gaussian vertex plate improves return loss and far-out sidelobes in prime-focus reflector antennas," *Microwave and Optical Technology Letters*, vol. 21, no. 2, pp. 125–129, 1999.